Journal of Molecular Graphics and Modelling 33 (2012) 26–34

Contents lists available at SciVerse ScienceDirect

Journal of Molecular Graphics and Modelling

journal homepage: www.elsevier.com/locate/JMGM

The origin of the unusual broad and intense visible absorption of tetrathiafulvalene-annulated zinc porphyrazine: A density functional theory study

Wei Tao[a], Yu-He Kan[a,b,*], Shui-Xing Wu[a], Hai-Bin Li[a], Li-Kai Yan[a], Shi-Ling Sun[a], Zhong-Min Su[a,*]

[a] Institute of Functional Material Chemistry, Faculty of Chemistry, Northeast Normal University, Changchun 130024, China
[b] Jiangsu Key Laboratory for Chemistry of Low-Dimensional Materials, School of Chemistry and Chemical Engineering, Huaiyin Normal University, Huaian 223300, People's Republic of China

ARTICLE INFO

Article history:
Received 18 June 2011
Received in revised form 26 October 2011
Accepted 27 October 2011
Available online 3 November 2011

Keywords:
Porphyrazine
Tetrathiafulvalene
Absorption spectra
Charge transfer
Time-dependent density functional theory

ABSTRACT

The vertical excitation energies of tetrathiafulvalene (TTF)-annulated zinc porphyrazine (ZnPzTTF) were investigated using time-dependent density functional theory (TDDFT) calculations and compared to the experimental UV–vis spectra. To examine the effects of the aza substitutions and TTF groups on the molecular properties, zinc complexes of porphyrin (ZnP), porphyrazine (ZnPz) and tetraTTF-annulated porphyrin (ZnPTTF) were also selected for comparison. It was shown that numerous electronic transitions with TTF-to-porphyrin or porphyrazine charge transfer character exist and the Q band of ZnPzTTF is dominated by TTF-to-porphyrazine charge transfer transition mixed with porphyrazine core unit itself except for classic porphyrazine $\pi \rightarrow \pi^*$ transitions. The Q band of ZnPzTTF mixes with other configurations, which breaks down the Gouterman's classic four-orbital model for the spectral interpretation. The data suggest that TDDFT/SAOP performs best for Q and B bands of ZnPzTTF with the maximum error in excitation energy being 0.17 eV. The CAM-B3LYP, ωB97XD and M06-2X calculations qualitatively predict that the low-lying electronic transitions of ZnPzTTF with TTF-to-porphyrazine charge transfer character located below the Q band. The broad and intense red-shifted Q band suggests that ZnPzTTF can be a candidate for dye-sensitized solar cells.

1. Introduction

Metal complexes of porphyrins, porphyrazines and their related tetrapyrrole ligands, have been of great importance as model compounds due to their biological functions such as photosynthesis, and as important functional materials in organic photoelectronic devices such as organic light-emitting diodes, organic photovoltaics and organic field-effect transistors [1]. The redox-active tetrathiafulvalene (TTF) is also an excellent π-electron donor with three different stable redox states (TTF, TTF^+, TTF^{2+}). TTF derivatives have been widely known as charge transporting and superconducting materials [2–4]. Recently, TTF-containing porphyrins [5–10], porphyrazines [11], phthalocyanines [12] and their analogues represent an exciting class of macrocyclic compounds because of their important applications such as electrochemical sensing of anions and second-order nonlinear optical (NLO)response. As to the photophysical properties, the absorption spectrum of the TTF-containing porphyrins shows a strong Soret band and two or three weak Q bands [6,9]. To our surprise, the absorption spectrum of the TTF-containing metalloporphyrazines or metallophthalocyanines shows a broad, red-shifted and intense Q band [11,12]. Experimentally, the appearance of the broad, red-shifted and intense Q band was attributed to a transition from the nonbonding sulfur and nitrogen electrons (n) to the porphyrazine (phthalocyanine) rings (π^*) ($n \rightarrow \pi^*$) and aggregation of the macrocyclic system. However, the origin of this intense Q band has not been demonstrated convincingly. The character of UV–vis spectra of TTF-containing metalloporphyrazines or metallophthalocyanines is similar to meso (ferrocenyl)-containing porphyrins [13,14] in which the redox-active ferrocene is also a good donor. The reasons for broadening of the Q band of the meso (ferrocenyl)-containing porphyrins could be the presence of ferrocene-centered molecular orbitals (MOs) located between the classic Gouterman-type porphyrin-centered π and π^* MOs ($\pi \rightarrow \pi^*$). So we hypothesize TTF-centered MOs are located between the Gouterman-type π and π^* MOs. Such a situation could potentially result in numerous TTF-to-porphyrazine (phthalocyanine) charge transfer transitions thus complicating the absorption spectra of the TTF-to-porphyrazine (phthalocyanine).

* Corresponding authors at: Institute of Functional Material Chemistry, Faculty of Chemistry, Northeast Normal University, Changchun 130024, China.
Tel.: +86 431 85099108; fax: +86 431 85684009.
E-mail addresses: yhkan@yahoo.cn (Y.-H. Kan), zmsu@nenu.edu.cn (Z.-M. Su).

1093-3263/$ – see front matter © 2011 Elsevier Inc. All rights reserved.
doi:10.1016/j.jmgm.2011.10.008

It is well recognized that density functional theory (DFT) and time-dependent DFT (TDDFT) methods have been employed successfully to explore both electronic structures and spectral properties on porphyrins and related tetrapyrrole ligands [15–26]. For example, Nguyen and Rosa carried out TDDFT/B3LYP and TDDFT/SAOP calculations on the excitation energies of zinc complexes of porphyrin (ZnP), porphyrazine (ZnPz) and phthalocyanine (ZnPc), respectively [15,16]. The results show that the TDDFT/SAOP results give satisfactory results. However, up to now, theoretical investigations on the photophysical properties of TTF-annulated metallotetrapyrroles were sparse. Our group has recently reported the electron spectra and second-order NLO properties of monoTTF–metalloporphyrins by means of DFT calculation [27].

In this paper, our initial interest focused on the ambiguous assignment of the electronic spectra of TTF-annulated tetrapyrrole derivatives. Here, in order to shed light on the role of tetraaza substitutions and tetraTTF annulations, electronic structure and absorption spectra of tetraTTF-annulated zinc porphyrazine (ZnPzTTF) and its parent compounds (tetraTTF-annulated zinc porphyrin (ZnPTTF), ZnPz and ZnP) were systematically investigated in detail using DFT and TDDFT calculations. In addition, we also employed some representative (meta)-hybrid functionals and long range corrected functionals in an attempt to explore the prediction of the low-lying CT states of ZnPzTTF. TDDFT results suggest that the Q band of ZnPzTTF are dominated by TTF-to-porphyrazine charge transfer character mixed with porphyrazine core unit itself except for classic porphyrazine $\pi \rightarrow \pi^*$ transitions and conformational inhomogeneity is also likely to contribute to the broadening of the Q band of ZnPzTTF to some extent. ZnPzTTF is able to harvest light over a wide spectral range, so they are potential sensitizers for dye-sensitized solar cells (DSSCs). We hope that our investigation of the electronic spectra of TTF-annulated tetrapyrrole derivatives can provide guidance to the design novel tetrapyrrole sensitizers for DSSCs.

2. Computational details

The models of ZnP, ZnPz, ZnPTTF and ZnPzTTF are shown in Fig. 1. The ground state geometry of the four complexes was optimized at the DFT/BP86 level [28,29] using ADF2008.01 program [30–32] with triple-ξ plus polarization Slater-type orbital basis sets (TZP). The numerical integration of 6.0 and the scalar relativistic effects via the zero-order regular approximation (ZORA) [33] have been used to provide accurate results. Vertical singlet excitation energies and oscillator strengths of the lowest dipole and spin allowed excited states of the four complexes were calculated at the scalar relativistic TDDFT level using the asymptotically correct statistical-average-of-orbital potentials (SAOP) [34,35] along with the TZP basis sets. SAOP is widely and reliably used for the prediction of electronic structures and absorption spectra of porphyrins and related tetrapyrrole ligands [16,18,19,22,23,36,37]. The solvation was modeled through the conductor-like screening model (COSMO) [38,39] as implemented in ADF programs [40] with chloroform as solvent.

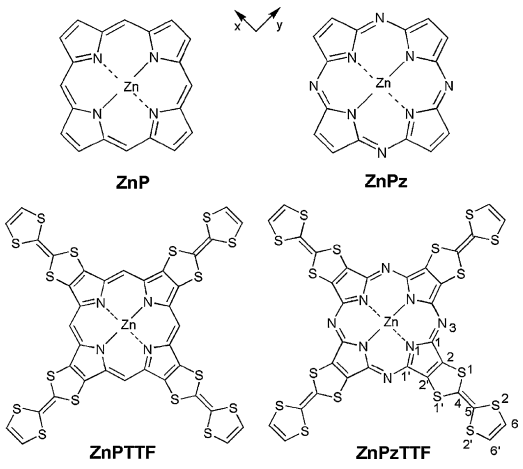

Fig. 1. Molecular structures of ZnP, ZnPz, ZnPTTF and ZnPzTTF.

The theoretical description of the absorption spectra of ZnPTTF and ZnPzTTF is complicated due to the introduction of charge transfer excited states upon incorporation of TTF units. In general, the conventional TDDFT methods notoriously underestimate the excitation energy of charge transfer (CT) transitions [41–43]. To this end, we also performed geometric optimization and frequency analysis of ZnPzTTF at DFT/PBE0 level [44] using Gaussian09 program [45] with 6-31G* basis set for C, H, O, N, S and def2-TZVP basis set [46] for zinc atom. In particular, based on the optimized ZnPzTTF geometry, vertical singlet excitation energies were calculated using PBE0, B3LYP [47–49], LC-ωPBE [50–53], CAM-B3LYP [54], ωB97XD [55], M06-HF [56,57] and M06-2X [58], because the hybrid functionals (PBE0 and B3LYP) with some fraction of the non-local Hartree–Fock (HF) exchange can alleviate, partly or satisfactorily, the CT problem of TDDFT. Recently, the long-range corrected (LC) functionals (LC-ωPBE, CAM-B3LYP and ωB97XD) was widely and accurately used to improve the CT states in porphyrins [17,20,59]. M06-HF is a full Hartree–Fock exchange functional with adapting to long-range properties and that performs well for Rydberg and CT excitations. M06-2X with double amount of nonlocal exchange was designed for valence and Rydberg excitations. The solvent effect of chloroform was simulated using the integral equation formalism of the polarized continuum model (IEFPCM) in Gaussian suite of program [60].

Molecular orbital compositions were analyzed using the AOMix program [61,62] and the absorption spectra were simulated by the SWizard program [61,63] using the Gaussian model with a half-bandwidth of 4000 cm^{-1}.

3. Results and discussion

3.1. Geometrical structures

The geometrical structures of ZnP and ZnPz in the ground state were both optimized under D_{4h} symmetry [15]. The optimized geometries were subsequently verified to be local minima by frequency calculations. According to the crystal structure of analogous bisTTF–porphyrin [9], where the TTF fragments are bowed, C_s, C_{2h}, C_{4v} and D_{2d} symmetry structure of ZnPzTTF were checked (Fig. S1). The lowest energy was found for the C_{4v} conformer, though the energy difference between other conformers was found to be small in the range of 0.01–0.65 kcal/mol (Table 1). The frequency calculations showed that the C_{2h} and C_{4v} structures are true minima (all positive frequencies) and that the C_s and D_{2d} structures contain imaginary frequencies and hence are not local minima (Supporting information pp. S5–S15). Therefore, the C_{4v} structure of ZnPTTF and ZnPzTTF is mainly considered. These four molecules lay in the *xy* plane with the *x* and *y* axes passing through pyrrolic nitrogens (Fig. 1). The selected optimized structure data at BP86 and PBE0 level are summarized in Table 2, and the available experimental values of ZnP are also included.

Table 1
Relative energies ΔEr (in kcal/mol) of the ZnPzTTF conformers calculated by BP/TZP.

Symmetry	C_{4v}	C_{2h}	C_s	D_{2d}	D_{4h}
ΔE_r	0	0.01	0.16	0.22	0.65

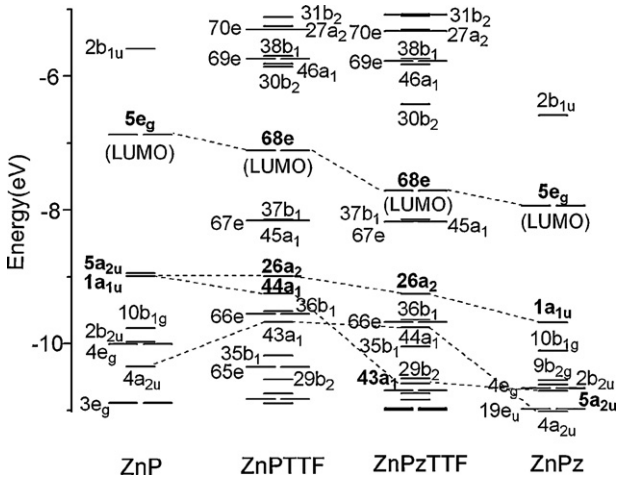

Fig. 2. Energy level schemes for ZnP, ZnPz, ZnPTTF and ZnPzTTF calculated by SAOP.

As evident from Table 2, the calculated structural data are in good agreement with the available experiment result. The deviations of the bond lengths of ZnP are less than 0.020 Å. The bond angles of ZnP agree well with experimental values. We note that the C_1–N_3 bond of ZnPz shorten by 0.058 Å in comparison with ZnP, which leads to a reduction of the size of the central hole because of the nitrogen substitutions at the four *meso* positions. The same tendency has also been reported by Nguyen and Pachter [15]. The maximum difference of the bond lengths between ZnP and ZnPTTF is 0.006 Å, and the maximum difference of the bond angles is 0.5°. Compared to ZnPz, the variation of the bond lengths and angles of ZnPzTTF is also negligible. These observations indicate that tetraTTF annulations wave little influence on the structure of the tetrapyrrolic rings.

The effect on the optimized geometries of ZnPzTTF caused by the two different functionals (BP86 and PBE0) is small. The differences of the bond lengths are less than 0.014 Å and the deviations of the bond angles are less than 0.5°.

3.2. Electronic structure

Metalloporphyrin-like systems show two UV–vis absorption bands, which are intense absorption, so-called near-ultraviolet Soret or B bands, followed by weaker absorption, known as visible Q bands. In terms of the Gouterman's four-orbital model [64–66], the principal excitations of B and Q bands involve a pair of highest filled orbitals (quasidengerate a_{1u} and a_{2u}) and the lowest empty orbitals (doubly degenerate e_g). The model is based on the assumption of four energetically isolated Gouterman's orbitals. The transition dipole moments of $a_{1u} \rightarrow e_g$ and $a_{2u} \rightarrow e_g$ transitions are similar in magnitude and direction, leading to a strong intensity (B bands) transitions with high energy; while the weak intensity (Q bands) transitions are in opposite directions with low energy. Fig. 2 shows the energy levels of frontier molecular orbitals (FMOs) of four complexes at the SAOP/TZP level, and the electron density distributions of the important FMOs of four complexes are collected in Fig. S2 in Supplementary Information. In addition, the orbital compositions of ZnPTTF and ZnPzTTF in terms of zinc, porphyrin (porphyrazine) core and TTF are depicted in Fig. S3 in Supplementary Information.

In ZnP, the $5a_{2u}$ (HOMO) and $1a_{1u}$ (HOMO − 1) are quasi-degenerate orbitals, and the $5e_{g,xz}$ and $5e_{g,yz}$ (LUMOs) are doubly degenerate (Fig. 2). The four Gouterman's orbitals of ZnP are indeed isolated, with 4.18 eV separating them from the HOMO − 2 ($10b_{1g}$) and LUMO + 2 ($2b_{1u}$) orbitals, which supports the four-orbital Gouterman's model. In ZnPz, the N_3-based $5a_{2u}$ is not degenerate with the $1a_{1u}$, and it is even more stabilized (Fig. 2). Both $5e_g$ (LUMOs) and $1a_{1u}$ (HOMO) energies shift downwards, and LUMOs energies reduce with a larger extent, resulting in a decreased HOMO–LUMO gap for ZnPz. The four Gouterman's orbitals energy shifts are caused by tetraaza substitutions. The same tendency has been reported by Nguyen and Rosa et al. [15,16].

The direct annulation of the porphyrin core with four TTF units in ZnPTTF makes the four highest occupied molecular orbitals ($37b_1$, $67e_{xz}$, $67e_{yz}$ and $45a_1$) predominantly TTF-centered MOs while the classic porphyrin core-centered occupied π-orbitals ($26a_2$ and $44a_1$) are located at lower energies (Fig. 2; Supplementary Information Figs. S2 and S3). The energies of the TTF-based MOs shift up largely owing to introducing the excellent π-electron donor TTF units. However, the porphyrin core π-orbital contribution both shift downward to a small extent, and the $44a_1$ orbital decreases by a larger extent than the $26a_2$ orbital and this removes the quasi-degeneracy of two filled Gouterman's orbitals (Fig. 2). The two lowest unoccupied orbitals of ZnPTTF are still degenerate empty orbitals (doubly degenerate 67e) and predominantly porphyrin based Gouterman's type π* orbitals (Fig. 2; Supplementary Information Figs. S2 and S3). The energies decrease with the extension of the π system caused by tetraTTF-annulated porphyrin core, and they are energetically well separated from higher energy unoccupied orbitals (LUMO + 2). The other occupied $36b_1$, 66e and $43a_1$ orbitals of ZnPTTF with high energy correspond to the $2b_{2u}$, $4e_g$ and $4a_{2u}$ orbitals in ZnP and are mainly localized on both the TTF units and porphyrin core with larger population on the former unit than on the latter (Fig. 2; Supplementary Information Figs. S2 and S3). The energies of the $36b_1$, 66e and $43a_1$ orbitals increase due to introduction of the TTF fragments, so that they are close to the Gouterman's $44a_1$ orbital in energy. The near degeneracy of the $44a_1$ orbital with the other occupied orbitals gives rise to the complex structure of the Q and B regions in the spectra of ZnPTTF.

ZnPzTTF shows similar features to those of ZnPz and ZnPTTF, due to the effects of the aza substitutions and TTF groups on the frontier molecular orbitals of ZnP. As we expected, the four HOMOs of ZnPzTTF with large amplitude on the TTF increase by a large extent (Fig. 2; Supplementary Information Figs. S2 and S3) and lie between the Gouterman-type porphyrin-centered π and π* MOs. The two LUMOs decrease significantly (Fig. 2), which is influenced by a combination of tetraaza substitutions and tetraTTF annulations. These changes in the energy levels of HOMOs and LUMOs of ZnPzTTF lead to the smallest HOMO–LUMO gap of the four complexes (Fig. 2). The tetraaza substitutions and tetraTTF annulations on the porphyrin ring lead to a significant change in the FMOs of ZnPzTTF by generating new orbitals and lifting prior degeneracies. The alterations affect the electronic absorption spectral character, especially for the Q band. These points will be further demonstrated in detail in the following sections.

3.3. Electronic absorption spectra

3.3.1. Spectra for ZnP, ZnPz, ZnPTTF and ZnPzTTF

To observe the effects of aza bridges and TTF units on the excited-state properties of the basic porphyrinic ring, the absorption spectra of ZnP, ZnPz, ZnPTTF and ZnPzTTF were investigated using scalar relativistic TDDFT at the SAOP/TZP level of theory. Fig. 3 shows the simulated absorption spectra of the four complexes calculated by TDDFT/SAOP and experimental spectra. In order to clarify the electronic transition nature for absorption of these four complexes, the calculated excitation energies, oscillator strengths, and main configurations of the ^1E_u and ^1E states are collected in Table 2. Fig. 4 displays transitions between molecular orbitals for the four complexes, and gives some insight into the nature of Q and B bands.

Table 2
Optimized bond length (Å) and angles (°) for ZnP, ZnPz, ZnPTTF and ZnPzTTF.

	BP86				PBE0
	ZnP (D_{4h})	ZnPz (D_{4h})	ZnPTTF (C_{4v})	ZnPzTTF (C_{4v})	
Bond length					
$Zn–N_1$	2.052 (2.037)[a]	1.976	2.058	1.983	1.978
$N_1–C_1$	1.376 (1.376)	1.373	1.382	1.381	1.367
$C_1–C_2$	1.447 (1.440)	1.461	1.442	1.451	1.447
$C_2–C_2$	1.367 (1.349)	1.364	1.373	1.376	1.367
$C_1–C_3(N_3)$	1.397 (1.400)	1.339	1.393	1.334	1.326
Bond angles					
$Zn–N_1–C_1$	126.6 (126.3)	125.8	126.2	125.5	125.4
$C_2–C_1–C_3(N_3)$	125.3 (125.0)	123.8	125.6	124.1	124.2
$N_1–C_1–C_3(N_3)$	125.0 (126.3)	127.5	125.5	127.9	127.8
$C_1–C_3(N_3)–C_1$	126.8 (124.7)	123.3	126.5	123.2	123.7

[a] Experimental values are taken from [67].

As displayed in Fig. 3, the absorption spectrum of the four complexes has two representative bands (Q and B bands) in the UV–vis region. It is noteworthy that the Q band of ZnPzTTF shows broadening and a bathochromic shift together with increased intensity relative to the Soret band. This character is significantly changed by the combination of tetraaza substitutions and tetraTTF annulations.

TDDFT/SAOP calculations have been previously shown to be effective for the prediction and assignment of electronic transitions in ZnP and ZnPz [16]. The present prediction of the Q and B bands of ZnP and ZnPz are mostly in excellent agreement with the experimental values with a maximum error in excitation energy of 0.05 eV. Only for the Q band of ZnPz, the computed value overestimates the excitation energy by 0.21 eV. As expected, the prediction of the most intense $\pi \rightarrow \pi^*$ transitions by TDDFT in the Q and Soret band regions of ZnP and ZnPz are in agreement with Gouterman's four orbital model and originate from a_{1u} and a_{2u} to $e_{g,xz}$ and $e_{g,xz}$ excitations (Table 3; Fig. 4).

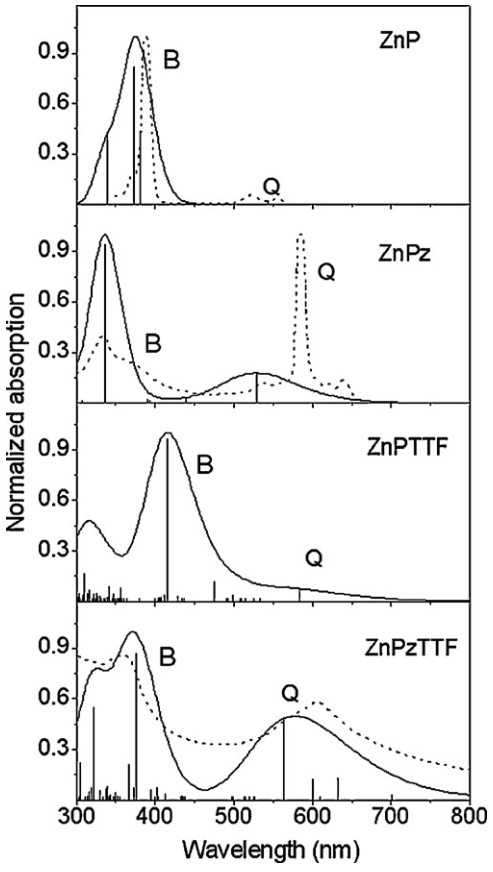

Fig. 3. Computed (TDDFT/SAOP) electronic absorption spectrum in gas phase (solid line) and experimental spectrum (dashed line) of ZnP, ZnPz, ZnPTTF and ZnPzTTF.

For ZnPTTF, the presence of four predominant TTF-centered HOMO–HOMO – 3 molecular orbitals results in 1^1E and 2^1E states with TTF-to-porphyrin charge transfer character. These two states cannot be considered as the traditional red-shifted Q band of porphyrin derivatives. And that the oscillator strengths are small due to the little overlap between the two transition orbitals. In addition, two obvious states (8^1E and 10^1E state) were predicted by TDDFT between the Q and the Soret bands. The two states arise from $36b_1$ to 68e (92%) and $43a_1$ to 68e (87%), respectively. In terms of the electronic density populatioin of $36b_1$ and $43a_1$ of ZnPTTF as detailed above, the two states can be assigned to the transition of TTF-to-porphyrin charge transfer mixed with porphyrin core unit itself. The classic $\pi \rightarrow \pi^*$ Q band of ZnPTTF is assigned to the 3^1E state. In despite of the opposite directions of the two transition dipole moments ($26a_2 \rightarrow 68e$ and $44a_1 \rightarrow 68e$ transitions), the absorption of the Q band is obvious compared to ZnP due to the breakdown of the quasi-degeneracy of the $26a_2$ and $44a_1$ orbitals caused by tetraTTF annulations, which induces the transition dipole moments difference of the two transitions. On the other hand, the B band is assigned to the 14^1E state. The transitions give rise to the B band involve contributions from the $43a_1$ orbital which are mainly localized on both the TTF units and porphyrin core with larger distribution on the former unit than on the latter (Table 3; Fig. 4). This departs from the traditional four-orbital model. The Q and Soret bands of ZnPTTF all have red-shifts compared to ZnP due to the extension of the π system caused by tetraTTF-annulated porphyrin core.

As shown in Fig. 3, the Q band of ZnPzTTF is the broad and bathochromically shifted absorption band, which has a significantly increased intensity compared to the Soret band. They are predicted to lie at 1.96 eV, 2.07 eV and 2.20 eV, which are in excellent agreement with the experiment maximum absorption in chloroform solvent at 2.05 eV [11]. The Q band arises from the $26a_2 \rightarrow 68e$ transition (the Gouterman transition) with a main contribution from the $36b_1 \rightarrow 68e$ and $44a_1 \rightarrow 68e$ transitions (Table 3; Fig. 4). It is worth to note that $26a_2$ and 68e of ZnPzTTF almost completely come from $1a_{1u}$ and $5e_g$ of ZnPz, while the $36b_1$ and $44a_1$ orbitals of ZnPzTTF are localized on the TTF units and porphyrazine core with larger distribution on the former unit than on the latter (Supplementary Information Figs. S2 and S3). The transitions from $36b_1$ to 68e and $44a_1$ to 68e can be assigned to the transition of TTF-to-porphyrazine charge transfer mixed with porphyrazine core unit itself. As a result, the Q band is assigned to TTF-to-porphyrazine charge transfer transition mixed with porphyrazine core unit itself except for classic porphyrazine $\pi \rightarrow \pi^*$ transitions. Then, the B band is assigned to the 22^1E state. This band is predicted

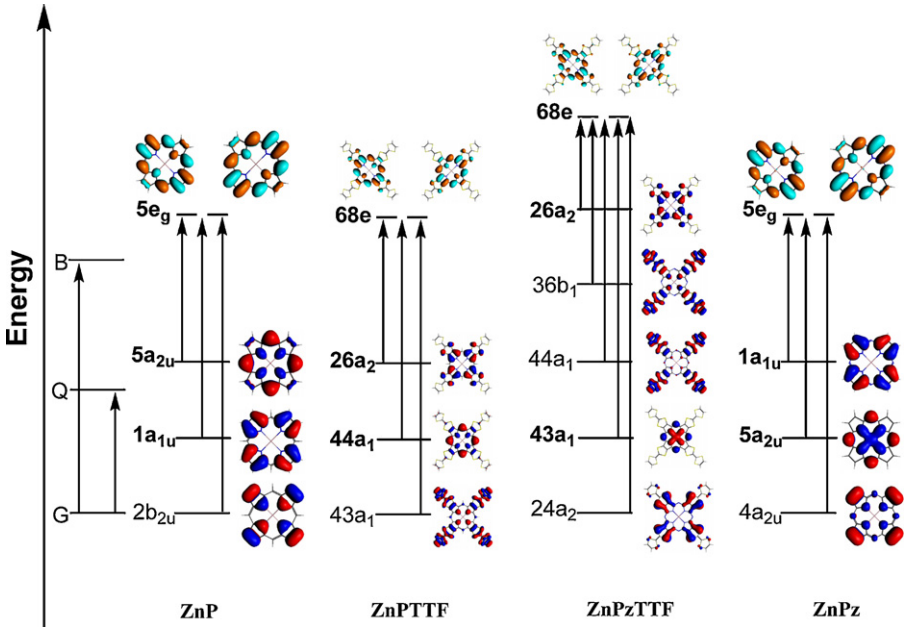

Fig. 4. Molecular transition orbital diagrams of ZnP, ZnPz, ZnPTTF and ZnPzTTF with corresponding simulated electron density maps calculated by SAOP/TZP. Energy is not to scale.

to appear at 3.30 eV with oscillator strength of 1.4429. These predicted excitation energies for the B band are in good agreement (within 0.17 eV) with the experiment values [11]. Note that the B band arises mainly from the $43a_1 \rightarrow 68e$ transition (the Gouterman transition) with a minor contribution from the $24a_2 \rightarrow 68e$ transitions. Furthermore, the $24a_2$ orbital mainly distributes on the donor TTF units. The nature of the B band can also be defined as the Gouterman transition along with charge transfer from donor TTF units to the porphyrazine ring (Table 3; Fig. 4). The combination of tetraaza substitutions and tetraTTF annulations not only influences the Q and B bands but also gives rise to the new and complex peaks (Table 3). The presence of four predominant TTF-centered HOMO–HOMO − 3 MOs in ZnPzTTF results in the 1^1E, 2^1E and 3^1E states with largely TTF-to-porphyrazine charge transfer character. The presence of predominant N_3-centered $29b_2$ MOs in ZnPzTTF results in 14^1E state with $n \rightarrow \pi^*$ character.

To get an insight into the effect of the solvent on the electronic excitation energies of the ZnPzTTF, Table 2 also shows the excitation energies of ZnPzTTF in chloroform. The effects of the solvent on the excitation energies of the representative Q and B bands are found to be negligible (within 0.06 eV). The calculated excitation energies of ZnPzTTF in chloroform reveals bathochromic shifts in Q and B bands compared with the excitation energies calculated in gas phase.

The motion from one C_{4v}-crown structure of ZnPzTTF to the opposite one through a planar D_{4h} structure has also been determined. Based on Ricciardi and Rosa et al. [71] stated, it is likely to flap from a saddled structure to the opposite one through a planar structure if the electronic transitions computed for the planar conformer were essentially identical in excitation energy, intensity and character to those computed for the saddled structure. Although the electronic transitions computed for the D_{4h} conformer of ZnPzTTF are appreciably different in absorption wavelength and intensity to those computed for the C_{4v} conformer, the shapes of the absorption spectrum of the two conformers are essentially identical (a half-bandwidth of 4000 cm^{-1}) (Fig. 5). Besides, the relative energy of D_{4h} conformer is a maximum of the five conformers, with four imaginary frequencies (Table 1; Supplementary Information pp. S5–S15). This indicates that the D_{4h} conformer is not stable and lasts short. Therefore, the flapping motion of the molecule from one crown conformation through the planar maximum to the opposite crown structure would not be detectable in the absorption spectrum.

The nature of the Q band of ZnPzTTF has been predicted in former section. Conformational inhomogeneity, which may contribute to the broadening of the Q band has also been considered. The simulated absorption spectra of the C_s, C_{2h}, D_{2d} and D_{4h} symmetry structures of ZnPzTTF at SAOP/TZP level have been collected in Fig. 5. It shows that the shapes of the absorption spectrum of the five conformers are nearly identical. C_s and C_{2h} symmetry structures are identical in absorption wavelength and intensity to the C_{4v} conformer. The wavelength of the Q band of D_{2d} conformer is appreciably red shift compared to the C_{4v} conformer, while the wavelength of the Q band of D_{4h} conformer shows appreciably blue shift compared to the C_{4v} conformer. Therefore, to some extent, conformational inhomogeneity is also likely to contribute to the broadening of the Q band of ZnPzTTF.

The effect of tetraTTF annulations on the absorption spectra of the unsubstituted zinc porphyrin is notable. The Q and Soret bands of ZnPTTF all have red-shifts with strong absorption in the Q

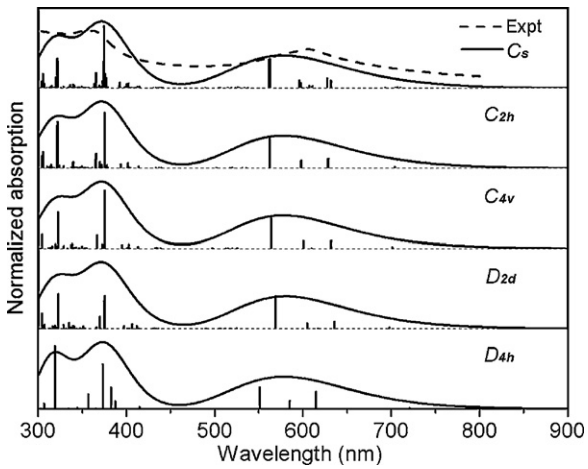

Fig. 5. Computed (TD-SAOP/TZP) electronic absorption spectrum in gas phase of C_s, C_{2h}, C_{4v}, D_{2d} and D_{4h} symmetry structure of ZnPzTTF.

Table 3
Calculated excitation energies and oscillator strengths (*f*) of ZnP, ZnPz, ZnPTTF, and ZnPzTTF in the gas phase and ZnPzTTF in the chloroform compared with experimental data calculated by SAOP.

State	Composition (%)	E^{exc},eV(nm)			Assignment
		Calc.	Expt.	*f*	
ZnP					
1^1E_u	51(**$5a_{2u}$** → **$5e_g$**); 47(**$1a_{1u}$** → **$5e_g$**)	2.28 (544)	2.23[a], 2.18[X]	0.0024	π → π* (Q)
2^1E_u	68($2b_{2u}$ → **$5e_g$**); 18(**$1a_{1u}$** → **$5e_g$**); 10(**$5a_{2u}$** → **$5e_g$**)	3.25 (382)	3.18[a], 3.13[b]	0.4968	π → π*
3^1E_u	31(**$5a_{2u}$** → **$5e_g$**); 30($2b_{2u}$ → **$5e_g$**); 27(**$1a_{1u}$** → **$5e_g$**)	3.32 (373)	3.35[a]	0.9504	π → π* (B)
ZnPz					
1^1E_u	78(**$1a_{1u}$** → **$5e_g$**); 19(**$5a_{2u}$** → **$5e_g$**)	2.34 (530)	2.13[c]	0.2554	π → π* (Q)
2^1E_u	97($2b_{2u}$ → **$5e_g$**)	2.82 (439)		0.0241	π → π*
3^1E_u	76($4a_{2u}$ → **$5e_g$**); 21(**$5a_{2u}$** → **$5e_g$**)	3.17 (391)	3.44[c]	0.0120	π → π* (B)
4^1E_u	57(**$5a_{2u}$** → **$5e_g$**); 18($4a_{2u}$ → **$5e_g$**); 17(**$1a_{1u}$** → **$5e_g$**)	3.69 (336)	3.73[c]	1.4463	
ZnPTTF					
1^1E	98($37b_1$ → **68e**)	1.07 (1158)		0.0332	TTF → P CT
2^1E	97 ($45a_1$ → **68e**)	1.10 (1129)		0.0543	TTF → P CT
3^1E	63(**$26a_2$** → **68e**); 34(**$44a_1$** → **68e**)	2.13 (583)		0.1926	π → π* (Q, P)
8^1E	92($36b_1$ → **68e**)	2.49 (498)		0.0517	TTF → P CT π → π* (P)
10^1E	87($43a_1$ → **68e**)	2.62 (474)		0.2921	TTF → P CT π → π* (P)
14^1E	51(**$44a_1$** → **68e**); 25(**$26a_2$** → **68e**); 11($43a_1$ → **68e**)	2.99 (415)		2.8140	π → π* (B, P) TTF → P CT
ZnPzTTF					
1^1E	73($37b_1$ → **68e**); 27($45a_1$ → **68e**)	0.50 (2510)		0.0020	TTF → Pz CT
2^1E	72($45a_1$ → **68e**); 27($37b_1$ → **68e**)	0.58 (2151)		0.1833	TTF → Pz CT
3^1E	87(67e → $30b_2$); 11(**$26a_2$** → **68e**)	1.77 (701)		0.0261	TTF → Pz CT
4^1E	64($36b_1$ → **68e**); 22(**$26a_2$** → **68e**); 11($44a_1$ → **68e**)	1.96 (632)	2.05[d]	0.1947	π → π* (Q, Pz)
5^1E	36($44a_1$ → **68e**); 32($36b_1$ → **68e**); 21(**$26a_2$** → **68e**)	2.07 (600)		0.1822	TTF → Pz CT
6^1E	51($44a_1$ → **68e**); 36(**$26a_2$** → **68e**)	2.20 (564)		0.7787	
14^1E	99($29b_2$ → **68e**)	2.86 (434)		0.0083	n → π*
21^1E	90($25a_2$ → **68e**)	3.14 (395)		0.0792	TTF → Pz CT
22^1E	64(**$43a_1$** → **68e**); 11($24a_2$ → **68e**)	3.30 (375)	3.47[d]	1.4429	π → π* (B, Pz) TTF → Pz CT
23^1E	90(66e → $30b_2$)	3.33 (373)		0.0986	TTF → Pz CT
ZnPzTTF (in the chloroform)					
1^1E	68($37b_1$ → **68e**); 32($45a_1$ → **68e**)	0.43 (2889)		0.0008	TTF → Pz CT
2^1E	68($45a_1$ → **68e**); 31($37b_1$ → **68e**)	0.53 (2324)		0.1995	TTF → Pz CT
3^1E	87(67e → $30b_2$); 11(**$26a_2$** → **68e**)	1.71 (726)		0.0151	TTF → Pz CT
4^1E	76($36b_1$ → **68e**); 14(**$26a_2$** → **68e**)	1.90 (652)	2.05[d]	0.1206	π → π* (Q, Pz)
5^1E	58($44a_1$ → **68e**); 20($36b_1$ → **68e**); 14(**$26a_2$** → **68e**)	2.01 (618)		0.0920	TTF → Pz CT
6^1E	51(**$26a_2$** → **68e**); 31($44a_1$ → **68e**)	2.17 (573)		0.9668	
12^1E	99($29b_2$ → **68e**)	2.92 (425)		0.0336	n → π*
22^1E	91(66e → $30b_2$)	3.25 (381)		0.0165	TTF → Pz CT
23^1E	69(**$43a_1$** → **68e**); 10($24a_2$ → **68e**)	3.30 (376)	3.47[d]	1.3574	π → π* (B, Pz) TTF → Pz CT

[a] Data taken in *n*-octane, from Ref. [68].
[b] Data taken in MeOH, from Ref. [69].
[c] Ref. [70].
[d] Ref. [11].

band. Moreover, the Soret band mixes with the contributions from the $43a_1$ orbital, which breaks down the traditional four-orbital model. Similarly, the transitions of ZnPzTTF are more complex than that of ZnPTTF. The Q band of ZnPzTTF shows remarkably broad and intense absorption. The Q band also involves contributions from the $36b_1$ and $44a_1$ orbitals besides the Gouterman orbital ($26a_2$), thus the transition of the Q band is assigned to TTF-to-porphyrazine charge transfer character mixed with porphyrazine core unit itself except for classic porphyrazine π → π* transitions. Conformational inhomogeneity is also likely to contribute to the broadening of the Q band of ZnPzTTF to some extent.

3.3.2. Hybrid and long-range corrected functionals exctied states of ZnPzTTF

Taking ZnPzTTF as an example, TDDFT/SAOP yields fairly accurate results for non-CT valence-excited states (Q and B bands). However, within the typical TDDFT errors, the vertical excitation energies of the low-lying CT transitions are underestimated by the TDDFT method, which prevents the correct assignment of some spectral features [43]. So, we also employ PBE0, B3LYP, LC-ωPBE, CAM-B3LYP, ωB97XD, M06-HF and M06-2X to investigate the low-lying CT states of ZnPzTTF at the PBE0 optimized geometry. Table 4 and Table S1 show excitation energies and oscillator strength of the former ten excited states ZnPzTTF obtained from the seven functionals in the gas phase and in chloroform. The solvent effect on the excitation energies of the low-lying CT and Q bands is still found to be small (within 0.08 eV).

For functional SAOP, PBE0 and B3LYP, the CT bands of ZnPzTTF lie below the Q bands (Table 2). The two low-lying CT bands lie at the near-infrared region and the CT transition energies are underestimated notablely. For functional M06-2X and CAM-B3LYP, the CT states also lie below the Q band and the excitation energies of the CT states are largely improved. However, for the Q band of ZnPzTTF, the M06-2X and CAM-B3LYP results are poor to experiment (with 0.28–0.30 eV). The ωB97XD result shows that the Q band lies between the two CT states and the excitation energies of the CT states are also largely improved. Interestingly, the LC-ωPBE and M06-HF calculations are substantially different from the above functionals, and the CT bands lie above the Q band. For the Q band, ωB97XD, LC-ωPBE and M06-HF results are closer to experiment (within 0.11 eV). The ωB97XD gives the best result for the Q_y band, which is supported by studies on Pd-bacteriopheophorbide (Pd-BPheid) and metal-free BPheid [20]. As Dreuw and Head-Gordon depicted [42], in oligomeric tetrapyrrol systems, the excited Q-states can, in principle, decay

Table 4
Calculated excitation energies (eV) and oscillator strengths (in parentheses) of ZnPzTTF calculated by different functionals in the gas phase.

State	E_{exc}, eV(nm)	f	Assignment
PBE0			
1^1E	1.09 (1134)	0.0010	TTF → Pz CT
3^1E	1.19 (1039)	0.1710	TTF → Pz CT
5^1E	2.31 (537)	1.0562	$\pi \rightarrow \pi^*$ (Q)
B3LYP			
1^1E	1.01 (1230)	0.0002	TTF → Pz CT
3^1E	1.09 (1137)	0.1682	TTF → Pz CT
5^1E	2.28 (545)	0.9510	$\pi \rightarrow \pi^*$ (Q)
LC-ωPBE			
1^1E	1.96 (633)	0.5310	$\pi \rightarrow \pi^*$ (Q)
3^1E	2.40 (517)	0.2074	TTF → Pz CT
5^1E	2.94 (422)	1.0410	TTF → Pz CT
CAM-B3LYP			
1^1E	1.78 (696)	0.0000	TTF → Pz CT
3^1E	2.02 (613)	0.0004	TTF → Pz CT
5^1E	2.33 (533)	1.4594	$\pi \rightarrow \pi^*$ (Q)
ωB97XD			
1^1E	1.92 (646)	0.0270	TTF → Pz CT
3^1E	2.16 (575)	0.2668	$\pi \rightarrow \pi^*$ (Q)
5^1E	2.46 (504)	1.2764	TTF → Pz CT $\pi \rightarrow \pi^*$[a]
M06-HF			
1^1E	2.10 (591)	0.5864	$\pi \rightarrow \pi^*$ (Q)
3^1E	2.52 (493)	0.1914	TTF → Pz CT
5^1E	3.10 (401)	1.0526	TTF → Pz CT
M06-2X			
1^1E	1.65 (751)	0.0018	TTF → Pz CT
3^1E	1.88 (660)	0.0792	TTF → Pz CT
5^1E	2.35 (527)	1.3846	$\pi \rightarrow \pi^*$ (Q)

[a] The transition is caused by the Gouterman's orbitals.

nonradiatively into the CT states if low-lying charge transfer (CT) excited states lie energetically below the Q states. Moreover, the process corresponds to electron-transfer quenching of the excited-state fluorescence. Experimentally, the fluorescence quenching has been observed in monoTTF–porphyrin [9]. This suggests that the CT states of ZnPzTTF lie well below the Q states. Hence, the CAM-B3LYP, M06-2X and ωB97XD calculations are qualitatively correct.

In conclusion, the CAM-B3LYP, M06-2X and ωB97XD calculations may correctly predict features of the CT states of ZnPzTTF. Especially, ωB97XD calculations also perform well on the Q band.

4. Conclusions

We have performed a detailed TDDFT analysis on the ground state structures and spectrum of tetraTTF-annulated zinc porphyrin and tetraTTF-annulated zinc porphyrazine. The calculations indicate that meso-tetraaza substitutions significantly reduce the central hole in ZnPz and ZnPzTTF compared to ZnP. Tetraaza substitutions and tetraTTF annulations invoke a large perturbation to both the nature and energy of the frontier molecular orbitals, which results in the generation of additional molecular orbitals from the parent metalloporphyrin species. The removing of the quasidegeneracy between the a_{1u} and a_{2u} orbitals induces the lifting of the near-degeneracy of the configurations ($a_{1u}e_g$) and ($a_{2u}e_g$) of the four-orbital model, which increases the intensity of the Q band. Moreover, the most intensive Q band is observed in ZnPzTTF. Additional electronic transitions arise from orbitals localized on the TTF groups. Numerous electronic transitions with TTF-to-porphyrin or porphyrazine charge transfer character are found and the Q band of ZnPzTTF is dominated by TTF-to-porphyrazine charge transfer transition mixed with porphyrazine core unit itself except for classic porphyrazine $\pi \rightarrow \pi^*$ transitions. Conformational inhomogeneity is also likely to contribute to the broadening of the Q band of ZnPzTTF to some extent. In solution the theoretical results indicated that it can flap from one C_{4v}-crown conformation of ZnPzTTF to the opposite one through a planar D_{4h} structure. ZnPzTTF has broad and red-shifted Q bands with enhanced intensity that may make this dye as a potential sensitizer for dye-sensitized solar cells.

Comparing results from different functionals, we conclude that SAOP provides more accurate excitation energies of Q and B bands of ZnPzTTF than other functionals. The CAM-B3LYP, M06-2X and ωB97XD calculations qualitatively predict that the low-lying electronic transitions with TTF-to-porphyrin or porphyrazine charge transfer character are localized below the Q band, which are in agreement with the experiment.

Acknowledgements

The authors gratefully acknowledge financial support from NSFC (Nos. 20903020), Chang Jiang Scholars Program (2006), Program for Changjiang Scholars and Innovative Research Team in University (IRT0714), National Basic Research Program of China (973 Program-2009CB623605), the Opening Project of Key Laboratory for Chemistry of Low-Dimensional Materials of Jiangsu Province (No. JSKC10082), and the Doctor Fund of HNU (HNU-08HSBSK004). We are also grateful to the reviewers for their critical and helpful comments on the manuscript.

Appendix A. Supplementary data

Supplementary data associated with this article can be found, in the online version, at doi:10.1016/j.jmgm.2011.10.008.

References

[1] K.M. Kadish, K.M. Smith, R. Guilard, The Porphyrin Handbook, San Diego, Academic Press, 2000.
[2] D. Lorcy, N. Bellec, Dithiadiazafulvalenes: promising precursors of molecular materials, Chem. Rev. 104 (2004) 5185–5202.
[3] C. Rovira, Bis(ethylenethio)tetrathiafulvalene (BET–TTF) and related dissymmetrical electron donors: from the molecule to functional molecular materials and devices (OFETs), Chem. Rev. 104 (2004) 5289–5318.
[4] Y.H. Kan, K. Wu, Y.L. Zhu, L.M. Hou, Z.M. Su, Charge transfer properties of fluorine-functionalized thieno-tetrathiafulvalene as organic field-effect materials, Acta. Phys. Chim. Sin. 26 (2010) 1423–1428.
[5] J. Becher, T. Brimert, J.O. Jeppesen, J.Z. Pedersen, R. Zubarev, T. Bjørnholm, N. Reitzel, T.R. Jensen, K. Kjaer, E. Levillain, Tetrathiafulvaleno-annelated porphyrins13, Angew. Chem. Int. Ed. 40 (2001) 2497–2500.
[6] H. Li, J.O. Jeppesen, E. Levillain, J. Becher, A mono-TTF-annulated porphyrin as a fluorescence switch, Chem. Commun. 84 (2003) 6–847.
[7] K.A. Nielsen, J.O. Jeppesen, E. Levillain, J. Becher, Mono-tetrathiafulvalene calix[4]pyrrole in the electrochemical sensing of anions, Angew. Chem. Int. Ed. 42 (2003) 187–191.
[8] K.A. Nielsen, W.S. Cho, J. Lyskawa, E. Levillain, V.M. Lynch, J.L. Sessler, J.O. Jeppesen, Tetrathiafulvalene-calix[4]pyrroles: synthesis, anion binding, and electrochemical properties, J. Am. Chem. Soc. 128 (2006) 2444–2451.
[9] K.A. Nielsen, E. Levillain, V.M. Lynch, J.L. Sessler, J.O. Jeppesen, Tetrathiafulvalene porphyrins, Chem. Eur. J. 15 (2009) 506–516.
[10] J.S. Park, F. Le Derf, C.M. Bejger, V.M. Lynch, J.L. Sessler, K.A. Nielsen, C. Johnsen, J.O. Jeppesen, Positive homotropic allosteric receptors for neutral guests: annulated tetrathiafulvalene–calix[4]pyrroles as colorimetric chemosensors for nitroaromatic explosives, Chem. Eur. J. 16 (2010) 848–854.
[11] F.S. Leng, R.B. Hou, L.Y. Jin, B.Z. Yin, R.G. Xiong, Synthesis, characterization and electrochemistry of the novel metalloporphyrazines annulated with tetrathiafulvalene having pentoxycarbonyl substituents, J. Porphyrins Phthalocyanines. 14 (2010) 108–114.
[12] C. Loosli, C. Jia, S.X. Liu, M. Haas, M. Dias, E. Levillain, A. Neels, G. Labat, A. Hauser, S. Decurtins, Synthesis and electrochemical and photophysical studies of tetrathiafulvalene-annulated phthalocyanines, J. Org. Chem. 70 (2005) 4988–4992.
[13] V.N. Nemykin, G.T. Rohde, C.D. Barrett, R.G. Hadt, C. Bizzarri, P. Galloni, B. Floris, I. Nowik, R.H. Herber, A.G. Marrani, R. Zanoni, N.M. Loim, Electron-transfer

processes in metal-free tetraferrocenylporphyrin. Understanding internal interactions to access mixed-valence states potentially useful for quantum cellular automata, J. Am. Chem. Soc. 131 (2009) 14969–14978.
[14] V.N. Nemykin, G.T. Rohde, C.D. Barrett, R.G. Hadt, J.R. Sabin, G. Reina, P. Galloni, B. Floris, Long-range electronic communication in free-base meso-poly(ferrocenyl)-containing porphyrins, Inorg. Chem. 49 (2010) 7497–7509.
[15] K.A. Nguyen, R. Pachter, Ground state electronic structures and spectra of zinc complexes of porphyrin, tetraazaporphyrin, tetrabenzoporphyrin, and phthalocyanine: a density functional theory study, J. Chem. Phys. 114 (2001) 10757–10767.
[16] E.J. Baerends, G. Ricciardi, A. Rosa, S.J.A. Van Gisbergen, A DFT/TDDFT interpretation of the ground and excited states of porphyrin and porphyrazine complexes, Coord. Chem. Rev. 230 (2002) 5–27.
[17] Z.L. Cai, M.J. Crossley, J.R. Reimers, R. Kobayashi, R.D. Amos, Density functional theory for charge transfer: the nature of the N-bands of porphyrins and chlorophylls revealed through CAM-B3LYP, CASPT2, and SAC-CI calculations, J. Phys. Chem. B 110 (2006) 15624–15632.
[18] M.P. Donzello, C. Ercolani, K.M. Kadish, G. Ricciardi, A. Rosa, P.A. Stuzhin, Tetrakis(thiadiazole)porphyrazines. 5. Electrochemical and DFT/TDDFT studies of the free-Base macrocycle and its MgII, ZnII, and CuI complexes, Inorg. Chem. 46 (2007) 4145–4157.
[19] M.P. Donzello, C. Ercolani, X. Cai, K.M. Kadish, G. Ricciardi, A. Rosa, Tetrakis(thiadiazole)porphyrazines. 6. Spectroelectrochemical and density functional theory studies of the anions $[TTDPzM]^{n-}$ ($n = 1$–4; M = Zn^{II}, $Mg^{II}(H_2O)$, Cu^{II}, $2H^{I}$), Inorg. Chem. 48 (2009) 9890–9903.
[20] B. Tian, E.S.E. Eriksson, L.A. Eriksson, Can range-separated and hybrid DFT functionals predict low-lying excitations? A tookad case study, J. Chem. Theor. Comput. 6 (2010) 2086–2094.
[21] Y.L. Zhu, S.Y. Zhou, Y.H. Kan, Z.M. Su, Electronic structures and spectra of porphyrin with fused benzoheterocycles: DFT and TDDFT–PCM investigations, Int. J. Quantum Chem. 107 (2007) 1614–1623.
[22] Y.L. Zhu, S.Y. Zhou, Y.H. Kan, L.K. Yan, Z.M. Su, Theoretical investigation of electronic structures and excitation energies of doubly N-confused porphyrin and its group 11 transition metal (III) complexes, J. Chem. Phys. 126 (2007) 245106–245108.
[23] Y.L. Zhu, S.Y. Zhou, Y.H. Kan, Z.M. Su, Theoretical investigation of electronic structures and excitation energies of hexaphyrin and its group 11 transition metal (III) complexes, J. Organomet. Chem. 694 (2009) 3012–3018.
[24] L. Wan, Y.X. Zhang, D.D. Qi, J.Z. Jiang, Structures and properties of 1,8,15,22-tetrasubstituted phthalocyaninato zinc and nickel complexes: substitution and axially coordination effects study based on density functional theory calculations, J. Mol. Graphics Modell. 28 (2010) 842–851.
[25] A.M. Zhong, Y.X. Zhang, Y.Z. Bian, Structures and spectroscopic properties of nonperipherally and peripherally substituted metal-free phthalocyanines: a substitution effect study based on density functional theory calculations, J. Mol. Graphics Modell. 29 (2010) 470–480.
[26] L.J. Zhang, D.D. Qi, Y.X. Zhang, Y.Z. Bian, J.Z. Jiang, Density functional theory studies on the structures and electronic communication of meso-ferrocenylporphyrins: long range orbital coupling via porphyrin core, J. Mol. Graphics Modell. 29 (2011) 717–725.
[27] C.G. Liu, W. Guan, P. Song, L.K. Yan, Z.M. Su, Redox-switchable second-order nonlinear optical responses of push–pull monotetrathiafulvalene–metalloporphyrins, Inorg. Chem. 48 (2009) 6548–6554.
[28] J.P. Perdew, Density-functional approximation for the correlation energy of the inhomogeneous electron gas, Phy. Rev. B 33 (1986) 8822.
[29] A.D. Becke, Density-functional exchange-energy approximation with correct asymptotic behavior, Phys. Rev. A 38 (1988) 3098.
[30] C. Fonseca Guerra, J.G. Snijders, G. Te Velde, E.J. Baerends, Towards an order-N DFT method, Theor. Chem. Acc. 99 (1998) 391–403.
[31] G. te Velde, F.M. Bickelhaupt, E.J. Baerends, C. Fonseca Guerra, S.J.A. van Gisbergen, J.G. Snijders, T. Ziegler, Chemistry with ADF, J. Comput. Chem. 22 (2001) 931–967.
[32] ADF2008.01, SCM, Theoretical Chemistry. Vrije Universiteit, Amsterdam, the Netherlands. Available at: http://www.scm.com, 2008.
[33] E. van Lenthe, E.J. Baerends, J.G. Snijders, Relativistic regular two-component Hamiltonians, J. Chem. Phys. 99 (1993) 4597–4610.
[34] O.V. Gritsenko, P.R.T. Schipper, E.J. Baerends, Approximation of the exchange-correlation Kohn–Sham potential with a statistical average of different orbital model potentials, Chem. Phys. Lett. 302 (1999) 199–207.
[35] P.R.T. Schipper, O.V. Gritsenko, S.J.A. van Gisbergen, E.J. Baerends, Molecular calculations of excitation energies and (hyper)polarizabilities with a statistical average of orbital model exchange-correlation potentials, J. Chem. Phys. 112 (2000) 1344–1352.
[36] A. Rosa, G. Ricciardi, E.J. Baerends, S.J.A. van Gisbergen, The optical spectra of NiP, NiPz, NiTBP, and NiPc: electronic effects of meso-tetraaza substitution and tetrabenzo annulation, J. Phys. Chem. A 105 (2001) 3311–3327.
[37] G. Ricciardi, A. Rosa, E.J. Baerends, Ground and excited states of zinc phthalocyanine studied by density functional methods, J. Phys. Chem. A 105 (2001) 5242–5254.
[38] A. Klamt, G. Schuurmann, COSMO. A new approach to dielectric screening in solvents with explicit expressions for the screening energy and its gradient, J. Chem. Soc. Perkin Trans. 2 (1993) 799–805.
[39] A. Klamt, V. Jonas, Treatment of the outlying charge in continuum solvation models, J. Chem. Phys. 105 (1996) 9972–9981.
[40] C.C. Pye, T. Ziegler, An implementation of the conductor-like screening model of solvation within the Amsterdam density functional package, Theor. Chem. Acc. 101 (1999) 396–408.
[41] A. Dreuw, J.L. Weisman, M. Head-Gordon, Long-range charge-transfer excited states in time-dependent density functional theory require non-local exchange, J. Chem. Phys. 119 (2003) 2943–2946.
[42] A. Dreuw, M. Head-Gordon, Failure of time-dependent density functional theory for long-range charge-transfer excited states: the zincbacteriochlorin–bacteriochlorin and bacteriochlorophyll–spheroidene complexes, J. Am. Chem. Soc. 126 (2004) 4007–4016.
[43] A. Dreuw, M. Head-Gordon, Single-reference ab initio methods for the calculation of excited states of large molecules, Chem. Rev. 105 (2005) 4009–4037.
[44] C. Adamo, V. Barone, Toward reliable density functional methods without adjustable parameters: the PBE0 model, J. Chem. Phys. 110 (1999) 6158–6170.
[45] M.J. Frisch, G.W. Trucks, H.B. Schlegel, G.E. Scuseria, M.A. Robb, J.R. Cheeseman, G. Scalmani, V. Barone, B. Mennucci, G.A. Petersson, H. Nakatsuji, M. Caricato, X. Li, H.P. Hratchian, A.F. Izmaylov, J. Bloino, G. Zheng, J.L. Sonnenberg, M. Hada, M. Ehara, K. Toyota, R. Fukuda, J. Hasegawa, M. Ishida, T. Nakajima, Y. Honda, O. Kitao, H. Nakai, T. Vreven, J.A. Montgomery Jr., J.E. Peralta, F. Ogliaro, M. Bearpark, J.J. Heyd, E. Brothers, K.N. Kudin, V.N. Staroverov, R. Kobayashi, J. Normand, K. Raghavachari, A. Rendell, J.C. Burant, S.S. Iyengar, J. Tomasi, M. Cossi, N. Rega, J.M. Millam, M. Klene, J.E. Knox, J.B. Cross, V. Bakken, C. Adamo, J. Jaramillo, R. Gomperts, R.E. Stratmann, O. Yazyev, A.J. Austin, R. Cammi, C. Pomelli, J.W. Ochterski, R.L. Martin, K. Morokuma, V.G. Zakrzewski, G.A. Voth, P. Salvador, J.J. Dannenberg, S. Dapprich, A.D. Daniels, O. Farkas, J.B. Foresman, J.V. Ortiz, J. Cioslowski, D.J. Fox, Gaussian 09, Revision A. 02, Gaussian, Inc., Wallingford, CT, 2009.
[46] F. Weigend, R. Ahlrichs, Balanced basis sets of split valence, triple zeta valence and quadruple zeta valence quality for H to Rn: design and assessment of accuracy, Phys. Chem. Chem. Phys. 7 (2005) 3297–3305.
[47] A.D. Becke, Density-functional thermochemistry. III. The role of exact exchange, J. Chem. Phys. 98 (1993) 5648–5652.
[48] C. Lee, W. Yang, R.G. Parr, Development of the Colle–Salvetti correlation-energy formula into a functional of the electron density, Phys. Rev. B 37 (1988) 785.
[49] B. Miehlich, A. Savin, H. Stoll, H. Preuss, Results obtained with the correlation energy density functionals of Becke and Lee, Yang and Parr, Chem. Phys. Lett. 157 (1989) 200–206.
[50] Y. Tawada, T. Tsuneda, S. Yanagisawa, T. Yanai, K. Hirao, A long-range-corrected time-dependent density functional theory, J. Chem. Phys. 120 (2004) 8425–8433.
[51] O.A. Vydrov, G.E. Scuseria, Assessment of a long-range corrected hybrid functional, J. Chem. Phys. 125 (2006) 234109.
[52] O.A. Vydrov, J. Heyd, A.V. Krukau, G.E. Scuseria, Importance of short-range versus long-range Hartree–Fock exchange for the performance of hybrid density functionals, J. Chem. Phys. 125 (2006) 074106–074109.
[53] O.A. Vydrov, G.E. Scuseria, J.P. Perdew, Tests of functionals for systems with fractional electron number, J. Chem. Phys. 126 (2007) 154109.
[54] T. Yanai, D.P. Tew, N.C. Handy, A new hybrid exchange-correlation functional using the Coulomb-attenuating method (CAM-B3LYP), Chem. Phys. Lett. 393 (2004) 51–57.
[55] J.D. Chai, M. Head-Gordon, Long-range corrected hybrid density functionals with damped atom-atom dispersion corrections, Phys. Chem. Chem. Phys. 10 (2008) 6615–6620.
[56] Y. Zhao, D.G. Truhlar, Comparative DFT study of van der Waals complexes: rare-gas dimers, alkaline-earth dimers, zinc dimer, and zinc-rare-gas dimers, J. Phys. Chem. A 110 (2006) 5121–5129.
[57] Y. Zhao, D.G. Truhlar, Density functional for spectroscopy: no long-range self-interaction error, good performance for rydberg and charge-transfer states, and better performance on average than B3LYP for ground states, J. Phys. Chem. A 110 (2006) 13126–13130.
[58] Y. Zhao, D. Truhlar, The M06 suite of density functionals for main group thermochemistry, thermochemical kinetics, noncovalent interactions, excited states, and transition elements: two new functionals and systematic testing of four M06-class functionals and 12 other functionals, Theor. Chem. Acc. 120 (2008) 215–241.
[59] N. Govind, M. Valiev, L. Jensen, K. Kowalski, Excitation energies of zinc porphyrin in aqueous solution using long-range corrected time-dependent density functional theory, J. Phys. Chem. A 113 (2009) 6041–6043.
[60] J. Tomasi, B. Mennucci, R. Cammi, Quantum mechanical continuum solvation models, Chem. Rev. 105 (2005) 2999–3094.
[61] S.I. Gorelsky, A.B.P. Lever, Electronic structure and spectra of ruthenium diimine complexes by density functional theory and INDO/S. Comparison of the two methods, J. Organomet. Chem. 635 (2001) 187–196.
[62] S.I. Gorelsky, AOMix Program for Molecular Orbital Analysis. Ottawa, Canada, 2009. Available at: http://www.sg-chem.net/.
[63] S.I. Gorelsky, SWizard Program. Ottawa, Canada, 2010. Available at: http://www.sg-chem.net/.
[64] M. Gouterman, Study of the effects of substitution on the absorption spectra of porphin, J. Chem. Phys. 30 (1959) 1139–1161.
[65] M. Gouterman, Spectra of porphyrins, J. Mol. Spectrosc. 6 (1961) 138–163.
[66] M. Gouterman, G.H. Wagnière, L.C. Snyder, Spectra of porphyrins: part II. Four orbital model, J. Mol. Spectrosc. 11 (1963) 108–127.
[67] W.R. Scheidt, J.U. Mondal, C.W. Eigenbrot, A. Adler, L.J. Radonovich, J.L. Hoard, Crystal and molecular structure of the silver(II) and zinc(II) derivatives of

meso-tetraphenylporphyrin. An exploration of crystal-packing effects on bond distance, Inorg. Chem. 25 (1986) 795–799.
[68] G.W. Canters, G. Jansen, M. Noort, J.H. van der Waals, High resolution Zeeman experiments on singlet, triplet, and quartet states of metalloporphines, J. Phys. Chem. 80 (1976) 2253–2259.
[69] H. Sekino, H. Kobayashi, A screened potential molecular-orbital calculation of the (-electron systems of metalloporphin, metallochlorin, and metallobacteriochlorin, J. Chem. Phys. 86 (1987) 5045–5052.
[70] S.S. Dvornikov, V.N. Knyukshto, V.A. Kuzmitsky, A.M. Shulga, K.N. Solovyov, Spectral-luminescent and quantum-chemical study of azaporphyrin molecules, J. Lumin. 23 (1981) 373–392.
[71] T.C. Gunaratne, A.V. Gusev, X.Z. Peng, A. Rosa, G. Ricciardi, E.J. Baerends, C. Rizzoli, M.E. Kenney, M.A.J. Rodgers, Photophysics of octabutoxy phthalocyaninato-Ni(II) in toluene: ultrafast experiments and DFT/TDDFT studies, J. Phys. Chem. A 109 (2005) 2078–2089.